

# Assembly of Defect-Free Microgel Nanomembranes for CO<sub>2</sub> Separation

Yu Hoshino,\* Tomohiro Gyobu, Kazushi Imamura, Akira Hamasaki, Ryutaro Honda, Ryoga Horii, Chie Yamashita, Yuki Terayama, Takeshi Watanabe, Shoma Aki, Yida Liu, Junko Matsuda, Yoshiko Miura, and Ikuo Taniguchi



Cite This: *ACS Appl. Mater. Interfaces* 2021, 13, 30030–30038



Read Online

ACCESS |

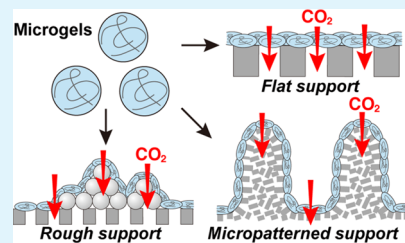
Metrics & More

Article Recommendations

Supporting Information

**ABSTRACT:** The development of robust and thin CO<sub>2</sub> separation membranes that allow fast and selective permeation of CO<sub>2</sub> will be crucial for rebalancing the global carbon cycle. Hydrogels are attractive membrane materials because of their tunable chemical properties and exceptionally high diffusion coefficients for solutes. However, their fragility prevents the fabrication of thin defect-free membranes suitable for gas separation. Here, we report the assembly of defect-free hydrogel nanomembranes for CO<sub>2</sub> separation. Such membranes can be prepared by coating an aqueous suspension of colloidal hydrogel microparticles (microgels) onto a flat, rough, or micropatterned porous support as long as the pores are hydrophilic and the pore size is smaller than the diameter of the microgels. The deformability of the microgel particles enables the autonomous assembly of defect-free 30–50 nm-thick membrane layers from deformed ~15 nm-thick discoidal particles. Microscopic analysis established that the penetration of water into the pores driven by capillary force assists the assembly of a defect-free dense hydrogel layer on the pores. Although the dried films did not show significant CO<sub>2</sub> permeance even in the presence of amine groups, the permeance dramatically increased when the membranes are adequately hydrated to form a hydrogel. This result indicated the importance of free water in the membranes to achieve fast diffusion of bicarbonate ions. The hydrogel nanomembranes consisting of amine-containing microgel particles show selective CO<sub>2</sub> permeation (850 GPU,  $\alpha_{\text{CO}_2/\text{N}_2} = 25$ ) against post-combustion gases. Acid-containing microgel membranes doped with amines show highly selective CO<sub>2</sub> permeation against post-combustion gases (1010 GPU,  $\alpha_{\text{CO}_2/\text{N}_2} = 216$ ) and direct air capture (1270 GPU,  $\alpha_{\text{CO}_2/\text{N}_2} = 2380$ ). The membrane formation mechanism reported in this paper will provide insights into the self-assembly of soft matters. Furthermore, the versatile strategy of fabricating hydrogel nanomembranes by the autonomous assembly of deformable microgels will enable the large-scale manufacturing of high-performance separation membranes, allowing low-cost carbon capture from post-combustion gases and atmospheric air.

**KEYWORDS:** deformable microgel, microgel membrane, micropatterned membrane, CO<sub>2</sub> separation, self-assembly



## INTRODUCTION

The development of efficient processes to capture, store, and/or utilize CO<sub>2</sub> will be indispensable for rebalancing the global carbon cycle.<sup>1–3</sup> The standard process for CO<sub>2</sub> capture is by chemical absorption using an aqueous amine solution. However, the process to regenerate the aqueous amine solution requires a high temperature, which has a high energy cost and therefore limits the use of this technique for carbon capture from gases with low CO<sub>2</sub> concentrations, such as post-combustion gases (~10 vol % CO<sub>2</sub>) and air (400 ppm CO<sub>2</sub>). Thus, it is important to develop materials and processes that do not require extra energy such as heat for the selective separation of CO<sub>2</sub>.

Membrane separation using CO<sub>2</sub>-permeable materials has been proposed as an energy-efficient approach for capturing CO<sub>2</sub> from low-concentration CO<sub>2</sub> gases.<sup>4–6</sup> Ideal membranes that show exclusive CO<sub>2</sub> permeation with negligible resistance theoretically enable complete CO<sub>2</sub> separation without heat. To achieve this ideal membrane separation, ultrathin membranes

without pinhole defects should be prepared using materials that allow rapid sorption, diffusion, and desorption of CO<sub>2</sub>.<sup>4</sup>

Hydrogels are viscoelastic solids comprising water and a network of polymeric molecules. These materials show exceptionally high solute diffusivity, comparable to that of liquids,<sup>7–9</sup> and are thus attractive materials for gas separation.<sup>10</sup> Moreover, the physicochemical properties of hydrogels can be tailored by introducing a variety of functional groups and modifying the cross-linking structure.<sup>11–13</sup> Furthermore, hydrogel-based materials can be used to capture CO<sub>2</sub> directly from

Received: April 8, 2021

Accepted: June 9, 2021

Published: June 18, 2021



humid gases such as post-combustion gases without a drying process.<sup>14</sup>

Recently, procedures to prepare defect-free nanomembranes from graphene oxide,<sup>15</sup> metal–organic frameworks,<sup>16</sup> polymers,<sup>17–19</sup> zeolites,<sup>20</sup> organic/inorganic interpenetrating networks,<sup>21</sup> and liquid water<sup>22</sup> have been reported. Functional hydrogels with nano/microarchitectures have been fabricated using photopatterning techniques,<sup>23</sup> self-assembly of building blocks,<sup>24</sup> and three-<sup>25,26</sup> and four-dimensional<sup>27</sup> printing techniques.<sup>28–30</sup> However, procedures to prepare defect-free hydrogel nanomembranes for CO<sub>2</sub> separation have seldom been reported.

In this study, we took advantage of the adaptability of colloidal hydrogel microparticles (microgels) to prepare defect-free hydrogel nanomembranes.<sup>31,32</sup> It has been reported that the deformability of ionized microgels enables the autonomous assembly of defect-free colloidal crystals, despite the broad size distribution of microgels.<sup>33,34</sup> Composite microgel membranes<sup>35–37</sup> and porous membranes coated with microgels<sup>38–43</sup> have been prepared as temperature-responsive functional membranes for water purification and enzymatic reactions. Furthermore, the affinity between microgels and CO<sub>2</sub> can be tuned by incorporating amine groups and/or by modulating the microenvironment around the amine groups in the microgels.<sup>11,12,44</sup> Thus, defect-free hydrogel nanomembranes for CO<sub>2</sub> separation could be obtained if the amine-containing microgels could be assembled on the surface of a porous support.

## RESULTS AND DISCUSSION

**Preparation of Microgel Nanomembranes on Flat Porous Supports.** Hydrogel nanomembranes were prepared by spray-coating the surface of a microporous membrane with an aqueous microgel suspension (Figure 1). Amine-containing

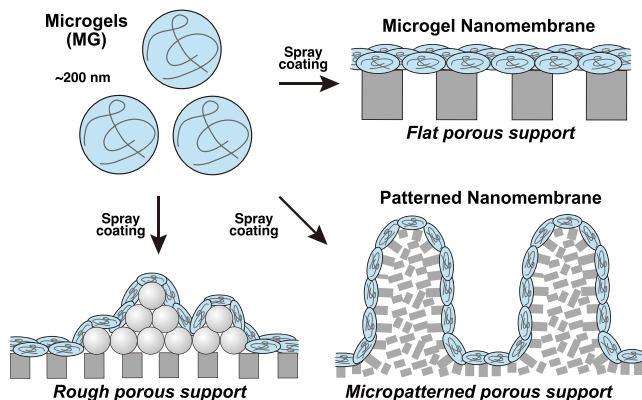
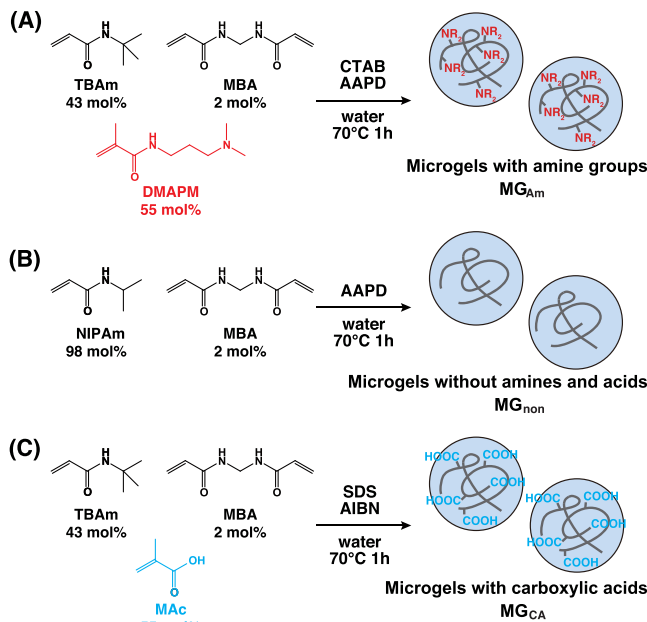


**Figure 1.** Assembly of defect-free hydrogel nanomembranes on flat, rough, and micropatterned porous supports by spray-coating a microgel (MG) suspension.

microgels (denoted as MG<sub>Am</sub>), which can absorb large amounts of CO<sub>2</sub>, were prepared by copolymerizing *N*-[3-(dimethylamino)propyl]methacrylamide (DMAPM, 55 mol %), *tert*-butyl acrylamide (TBAm, 43 mol %), and a small amount of a cross-linker *N,N'*-methylenebisacrylamide (MBA, 2 mol %) in an aqueous medium (Scheme 1).<sup>11</sup> The hydrodynamic diameter and polydispersity index (PDI) of MG<sub>Am</sub> are 235 nm and 0.106, respectively, as determined by dynamic light scattering (*Supporting Information*).

When the surface of a hydrophilic microporous polyether sulfone (PES) membrane with a nominal pore size of 100 nm

**Scheme 1. Synthesis of Microgels (A) with Amine Groups (MG<sub>Am</sub>), (B) without Amine or Acid Groups (MG<sub>non</sub>), and (C) with Carboxylic Acid Groups (MG<sub>CA</sub>)**



(denoted as PES<sub>100</sub>) was coated with the MG<sub>Am</sub> suspension (loading of 26 µg/cm<sup>2</sup>), the pore structure disappeared completely and a flat surface formed, as observed by scanning electron microscopy (SEM) (Figure 2A). The cross-sectional SEM image of the membrane indicates the formation of an ~200 nm-thick dense layer on the porous support (Figure 2B). This thickness is comparable to the thickness calculated (260 nm) based on the assumption that the MG<sub>Am</sub> layer has a density of 1 g/mL. On the other hand, MG<sub>Am</sub> could not form a defect-free flat layer on the surface of a microporous PES membrane with a nominal pore size of 450 nm (denoted as PES<sub>450</sub>), which is larger than the hydrodynamic diameter of MG<sub>Am</sub> (235 nm; Figure 2C).

Amine-containing microgels with a relatively smaller hydrodynamic diameter of 89 nm (denoted as MG<sub>Am-small</sub>; PDI = 0.176) and the non-cross-linked linear polymer (LP; M<sub>w</sub> = 72,000, PDI = 1.65) of DMAPM were prepared as control materials, as reported previously<sup>11,45</sup> (*Supporting Information*). When the same amounts (26 µg/cm<sup>2</sup>) of MG<sub>Am-small</sub> and LP were sprayed on PES<sub>100</sub> membranes, only a limited number of pores were filled, and a significant number of pores remained uncovered (Figure S1). Non-swollen solid polymethylmethacrylate (PMMA) particles with a diameter comparable to those of MG<sub>Am</sub> were also used as a control; when coated on PES<sub>100</sub> membranes, a porous layer with numerous interparticle cavities was formed (Figure 2D).

These results indicate that defect-free layers can be formed only when the hydrodynamic diameter of the swollen microgels is larger than the pore diameter of the supporting membrane. This is possibly because the microgels assemble on the surface without penetrating the pores of the support and subsequently deform during the drying process to form a dense layer.<sup>35–43</sup>

The gas-permeation behavior of the membranes (diameter = 25 mm) was investigated by flowing simulated post-combustion gases containing 10 vol % CO<sub>2</sub> and 90 vol % N<sub>2</sub> (95% relative humidity (RH), 40 °C, 100 mL/min) on the top side of the membranes (*Supporting Information*). The backside of the

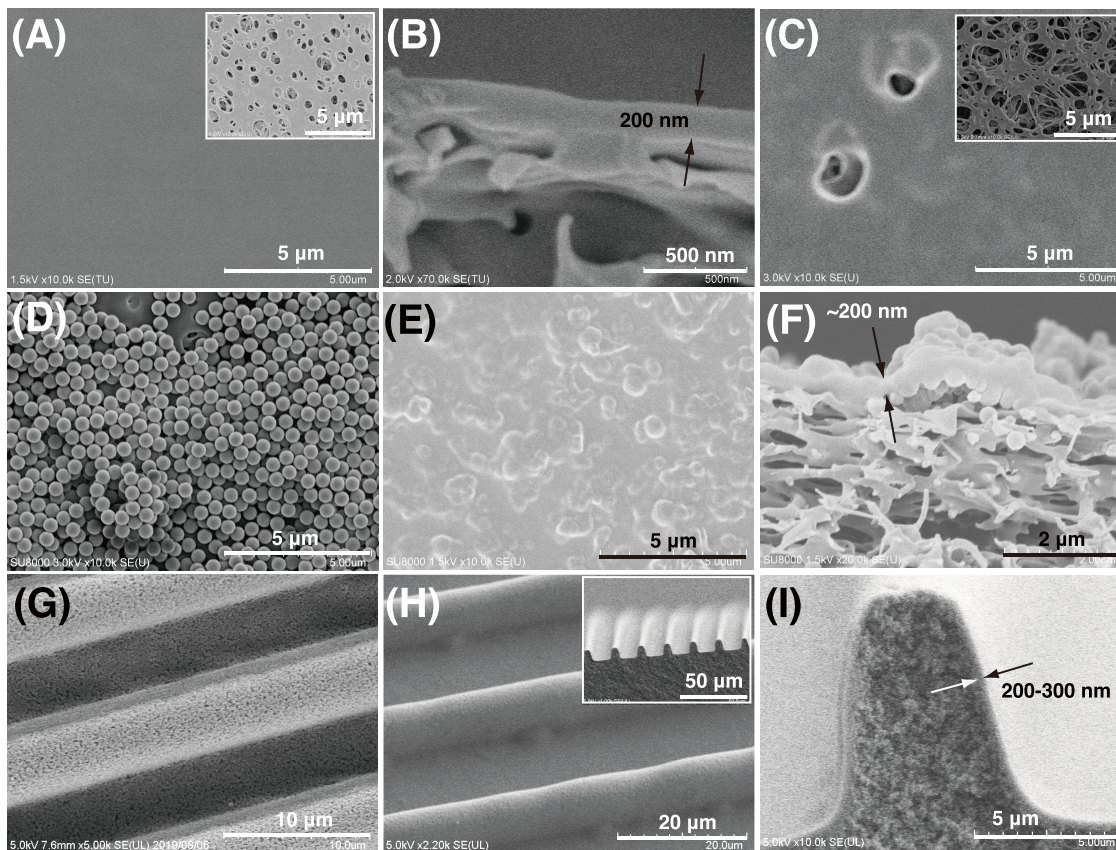


**Figure 2.** Surface and cross-sectional scanning electron microscopy (SEM) images of microporous polymer supports before and after coating with 235 nm diameter microgel particles or solid polymethylmethacrylate (PMMA) particles. (A) Surface and (B) cross section of the microgel-coated polyether sulfone membrane (pore size = 100 nm) ( $\text{PES}_{100}$ ). Inset: native  $\text{PES}_{100}$  membrane. (C) Surface of the microgel-coated  $\text{PES}_{450}$  membrane (pore size = 450 nm). Inset: native  $\text{PES}_{450}$  membrane. (D) Surface of the PMMA-coated  $\text{PES}_{100}$  membrane. (E) Surface and (F) cross section of the  $\text{PES}_{100}$  membrane covered with silica nanoparticle aggregates and then coated with the microgel. (G) Surface of native microporous membranes with a surface micropatterned by phase-separation micromolding. (H) Surface and (I) cross section of the micropatterned membranes coated with the microgel. Arrows in panels (B, F, I) indicate defect-free microgel layers.

membranes was swept with helium gas to quantify the amount of gaseous species in the permeate by gas chromatography. None of the membranes, except the  $\text{PES}_{100}$  membrane coated with  $\text{MG}_{\text{Am}}$ , showed selective  $\text{CO}_2$  permeation (Figure S2), indicating that the membranes did not function as  $\text{CO}_2$ -separation membranes. This may be because the membranes contained defects, as observed by microscopy analyses. On the other hand, the  $\text{PES}_{100}$  membrane coated with  $\text{MG}_{\text{Am}}$  (Figure 2A,B and Figure S2B) showed 100 times lower  $\text{N}_2$  permeability than the uncoated  $\text{PES}_{100}$  membrane (Figure S2B). Moreover, the relative concentration of  $\text{CO}_2$  in the permeate was much higher than that of the simulant gas on the top side of the membrane, indicating that the dense layer of  $\text{MG}_{\text{Am}}$  did not contain defects and thus functioned as a  $\text{CO}_2$ -separation membrane. The permeances of  $\text{CO}_2$  and  $\text{N}_2$  were calculated to be 189 gas permeation units (GPU, where 1 GPU =  $1 \times 10^{-6} \text{ cm}^3(\text{STP})/(\text{s} \cdot \text{cm}^2 \cdot \text{cm Hg})$ ) and 8.2 GPU, respectively. The  $\text{CO}_2$  selectivity ( $\alpha_{\text{CO}_2/\text{N}_2}$ , flux of  $\text{CO}_2$ /flux of  $\text{N}_2$ ) was 23.

**Preparation of Microgel Nanomembranes on Rough/Micropatterned Porous Supports.** The above-mentioned experiments established that defect-free hydrogel nanomembranes could be autonomously assembled on flat supports with pores. To demonstrate the versatility of the assembly process, silica nanoparticle aggregates were scattered on the porous support ( $\text{PES}_{100}$ ) by spray-coating a suspension of the silica nanoparticles before spray-coating of the  $\text{MG}_{\text{Am}}$  suspension (26

$\mu\text{g}/\text{cm}^2$ ). A 200–300 nm-thick  $\text{MG}_{\text{Am}}$  layer was assembled on the uneven surface of silica aggregates on the porous support (Figure 2E,F). The so-formed microgel membrane showed a  $\text{CO}_2$  permeance of 168 GPU and a selectivity ( $\alpha_{\text{CO}_2/\text{N}_2}$ ) of 28, indicating that defect-free membranes were successfully assembled on the surface of the rough porous support formed by depositing aggregates of silica particles (Figure 1).

In addition, a porous support with a patterned microstructure (5  $\mu\text{m}$  height, 5  $\mu\text{m}$  pitch, and line grating pattern) having a large effective surface area was prepared by polymerization-induced phase-separation micromolding of poly(2-ethylhexyl acrylate-*co*-ethylene glycol dimethacrylate) (Figure 2G).<sup>46,47</sup> Upon the spray-coating of  $\text{MG}_{\text{Am}}$  (52  $\mu\text{g}/\text{cm}^2$ ) on the patterned surface, the pores on the surface were completely covered by the microgel layer (Figure 2H), which had a thickness of 300 nm (Figure 2I). The so-formed microgel membrane showed a selective  $\text{CO}_2$  permeation of 395 GPU ( $\alpha_{\text{CO}_2/\text{N}_2} = 14$ ), which is approximately twice that of the microgel membrane assembled on a flat surface (201 GPU,  $\alpha_{\text{CO}_2/\text{N}_2} = 24$ ). These results reveal the versatility and potential of the assembly process in the fabrication of inexpensive high-performance microgel nanomembranes (Figure 1).

**Microscopic Analyses to Study the Membrane-Forming Mechanism.** For further analysis,  $\text{MG}_{\text{Am}}$  layers were formed on a track-etched polycarbonate (PC) membrane with uniform pores of 100 nm in diameter (denoted as  $\text{PC}_{100}$ ),

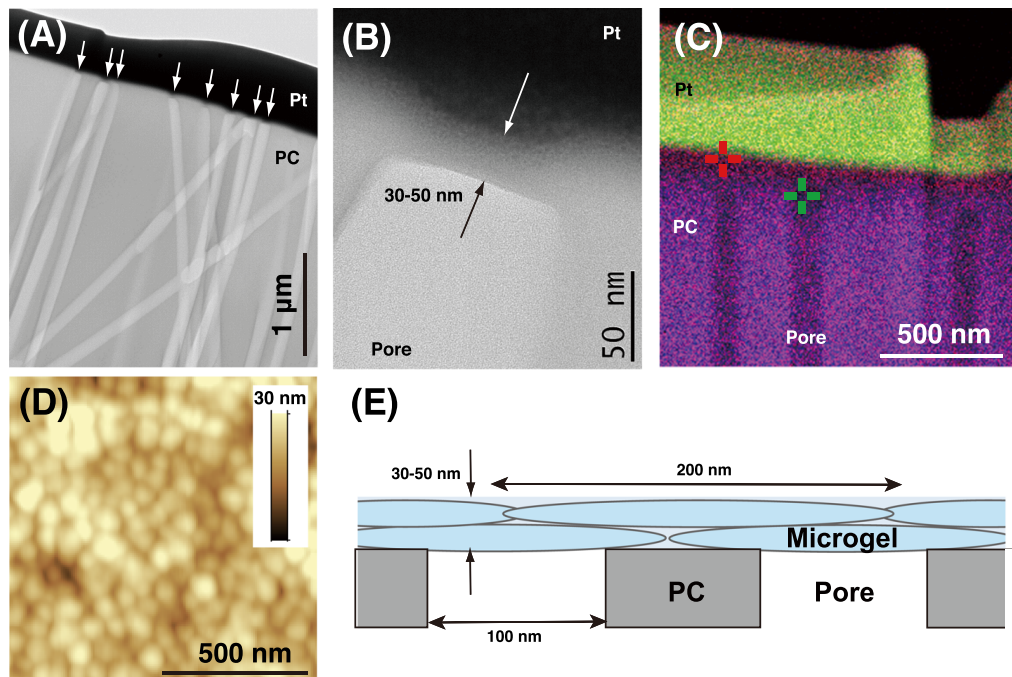


**Figure 3.** Assembly of hydrogel nanomembranes on the surface of a track-etched polycarbonate (PC) membrane with a uniform pore diameter (100 nm) and smooth surface, coated with 235 nm diameter microgels (MGs). (A) Transmission electron microscopy (TEM) image of cross-sectional slices of microgel-coated PC<sub>100</sub> ( $8.6 \mu\text{g}/\text{cm}^2$ ). Arrows indicate defect-free microgel layers, which prevent the diffusion of platinum into the pores. (B) TEM image of the microgel layer on the top of the pores in panel (A). Arrows indicate the microgel layer thickness. A platinum protective layer was deposited on the microgel layer before sectioning. (C) Energy-dispersive X-ray (EDX) spectroscopy mapping of cross-sectional slices of microgel-coated PC<sub>100</sub> ( $26 \mu\text{g}/\text{cm}^2$ ). Red, orange, green, and purple represent nitrogen, oxygen, platinum, and carbon, respectively. Nitrogen signals from microgels were observed in the position indicated by the red cross but not at the position indicated by the green cross. EDX maps of specific atoms and EDX spectra are shown in Figure S5. (D) Atomic force microscopy (AFM) image of the surface of the microgel layer. (E) Schematic of the hydrogel membranes consisting of two layers of discoidal microgels (blue ellipses) on porous PC<sub>100</sub> (gray).

which had a smoother surface than PES<sub>100</sub>. The MG<sub>Am</sub>-coated PC<sub>100</sub> membrane ( $8.6 \mu\text{g}/\text{cm}^2$ ) was protected with ion beam-deposited platinum, and cross-sectional slices were prepared using a focused ion beam for transmission electron microscopy (TEM) analysis and energy-dispersive X-ray (EDX) spectroscopy (Figure 3 and Figures S3–S5). The bright-field TEM image shows that deposited platinum was completely blocked by the MG<sub>Am</sub> layer on top of the pores (Figure 3A). The thickness of the MG<sub>Am</sub> layer was approximately 30–50 nm (Figure 3A). In the EDX analysis, nitrogen was detected in the thin layer on top of the pores (Figure 3C, red cross and Figure S5A,B) but not inside the pores (Figure 3C, green cross and Figure S5A,C), indicating that MG<sub>Am</sub> formed an active layer on top of the pores.

The atomic force microscopy (AFM) image (Figure 3D) of the surface of PC<sub>100</sub> coated with a 30–50 nm-thick layer of MG<sub>Am</sub> clearly shows discoidal particles with a root mean square roughness of 5.5 nm. Further, to observe the shape of a single microgel particle on the solid surface by AFM, a small amount of MG<sub>Am</sub> ( $0.01 \mu\text{g}/\text{cm}^2$ ) was coated on the PC<sub>100</sub> surface. MG<sub>Am</sub> adopted a discoidal form with a thickness of ~15 nm and a diameter of 200–300 nm, which is comparable to the measured hydrodynamic diameter of MG<sub>Am</sub> in the aqueous suspension (235 nm) (Figure S6). These results indicate that the defect-free 30–50 nm-thick membrane consists of two to three layers of deformed discoidal MG<sub>Am</sub> units (Figure 3E). The deformation of the discoidal units might have occurred at the air/water interface on the water droplet during the coating and/or drying process.<sup>48,49</sup>

As confirmed by the gas-permeation test, the 30–50 nm-thick defect-free MG<sub>Am</sub> layer could function as a CO<sub>2</sub> permeable

membrane; it exhibited a CO<sub>2</sub> permeance of 110 GPU and a selectivity ( $\alpha_{\text{CO}_2/\text{N}_2}$ ) of 25. This relatively low permeance might be due to the low surface porosity of the PC<sub>100</sub> membrane (porosity = 4.2%).<sup>50</sup> In fact, when the same particles (MG<sub>Am</sub>, 13  $\mu\text{g}/\text{cm}^2$ ) were coated on the surface of a highly porous alumina membrane (Anodisc; pore size = 100 nm, porosity = 29%),<sup>51</sup> a CO<sub>2</sub> permeance of 850 GPU ( $\alpha_{\text{CO}_2/\text{N}_2} = 25$ ) was observed. These results suggest the possibility of further improvement of the CO<sub>2</sub> permeability using porous support membranes with a high surface pore area and/or patterned microstructure.

When the amount of MG<sub>Am</sub> coated on PC<sub>100</sub> was decreased further, the N<sub>2</sub> flux increased and the selectivity ( $\alpha_{\text{CO}_2/\text{N}_2}$ ) decreased significantly, indicating that the pores on the membranes were not completely covered by MG<sub>Am</sub>. Indeed, SEM observations of the membrane surface indicated that not all the pores on the surface were covered by MG<sub>Am</sub> (Figure S7). However, interestingly, most of the pores on the surface were filled by MG<sub>Am</sub>, although the calculated thickness of MG<sub>Am</sub> on the surface was significantly lower than that of a single layer. These results indicate that a single particle of discoidal MG<sub>Am</sub> with a thickness of ~15 nm is enough to cover one pore, although a couple of layers are required to completely cover all the pores on the membrane without pinhole defects.

Further, the importance of the water penetration of the support membranes during the coating process was investigated by staining water and using hydrophilic and hydrophobic polyethylene (PE) membranes with 50 nm pores (PE<sub>50</sub>). A water-soluble red fluorescent dye (Rhodamine B) was dissolved in the coating suspension of the microgel, whereas the microgel particles themselves were labeled with a green fluorescent dye

(Fluorescein).<sup>14</sup> When the hydrophilic PE<sub>50</sub> membranes were coated by the microgel suspension (26  $\mu\text{g}/\text{cm}^2$ ), the microgel particles were observed only on the top portion of the membranes, although the penetration of Rhodamine B (red) in PE<sub>50</sub> (green) was confirmed by confocal laser scanning microscopy (CLSM) (Figure 4A). The coated defect-free

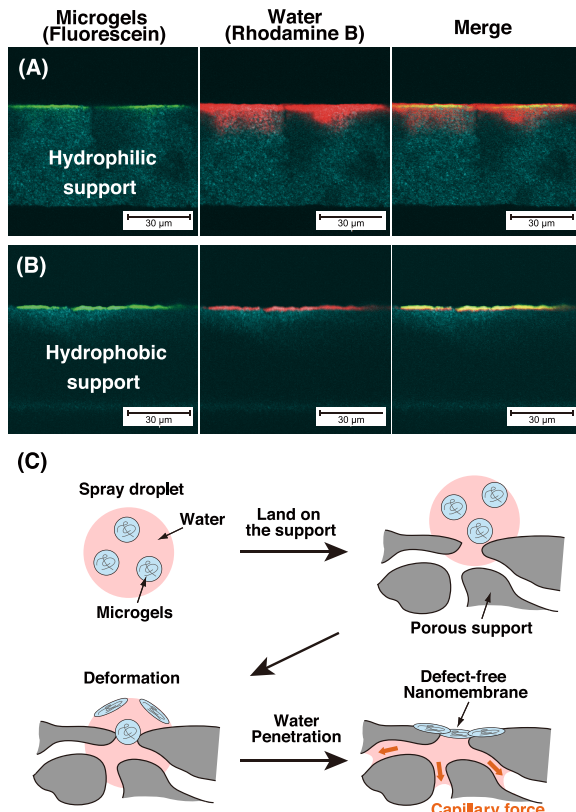


**Figure 4.** Effect of the hydrophobicity of the porous support membrane on the assembly of defect-free hydrogel nanomembranes. (A, B) Laser scanning microscopy image of the distribution of MGs (labeled with fluorescein, green) and penetrated water (labeled with Rhodamine B, red) in the cross section of hydrophilic (A) and hydrophobic (B) porous PE membranes (blue). (C) Schematic illustration of hydrogel membranes consisting of deformed discoidal MGs (blue ellipse) on the pores of PC<sub>100</sub> (gray).

membranes could be used for CO<sub>2</sub> gas separation when they exhibited a CO<sub>2</sub> permeance of 193 GPU and a selectivity ( $\alpha_{\text{CO}_2/\text{N}_2}$ ) of 20. On the other hand, when the same suspension was coated on the hydrophobic PE<sub>50</sub> membrane, which has the same pore structure as its hydrophilic counterpart, no penetration of the support membrane with Rhodamine B was observed (Figure 4B, red). Although the distribution of the microgel particles (Figure 4B, green) and surface morphology of the top part of the coated hydrophobic membranes were similar to those on the hydrophilic membrane (Figure S8), the resultant membrane showed low CO<sub>2</sub> selectivity ( $\alpha_{\text{CO}_2/\text{N}_2} = 9.1$ ) owing to the leakage of N<sub>2</sub> gas (23 GPU).

These results suggested that, during the coating process, the penetration of water was driven by capillary force, which assisted the autonomous assembly of a dense defect-free microgel layer on the pores. The water flux from the top to the bottom of the membranes would assist the particles to deform with respect to each other and thus plug the defects (Figure 4C). It has been reported that hydrogel particles are sometimes deformable

enough to pass through the pores of size much smaller than the particle diameter under the hydrodynamic pressure.<sup>52</sup> However, our microgels did not penetrate the pores in the spray-coating process; they instead remained on top of the pores (Figures 3 and 4). This is possibly because the force to deform the particles by the flux of water, which is driven by capillary forces in our process, is much smaller than that by hydrodynamic pressure used in a previous study (0.5 psi).<sup>52</sup>

### Mechanism of CO<sub>2</sub> Permeation through the Microgel Layer.

The CO<sub>2</sub> permeance of the MG<sub>Am</sub> membrane decreased significantly with decreasing RH (Figure 5A). As quantified with a quartz crystal microbalance, the amount of water in the MG<sub>Am</sub> layer decreased significantly upon reducing the RH (Figure 5B), indicating that the MG<sub>Am</sub> layer should be adequately hydrated to form a hydrogel during the separation process. On the other hand, hydrogel layers prepared from microgels without amine groups (Scheme 1) (denoted as MG<sub>non</sub>) showed much lower CO<sub>2</sub> permeance (7.5 GPU) and selectivity ( $\alpha_{\text{CO}_2/\text{N}_2} = 4$ ) even in the hydrated conditions (Figure 5A). These results indicate that amino groups as well as water are necessary for achieving high and selective CO<sub>2</sub> permeation. The difference of CO<sub>2</sub> permeance between two layers is due to different concentrations of absorbed CO<sub>2</sub> in each layer. The concentration of absorbed CO<sub>2</sub> (HCO<sub>3</sub><sup>-</sup>) in the top side of the MG<sub>Am</sub> membrane (feed gas side) is calculated to be about 0.2 M, assuming that the reaction between amines and CO<sub>2</sub> is equilibrated with the 10% (10 kPa) CO<sub>2</sub> feed gas and pK<sub>a</sub> of ammonium ions in MG<sub>Am</sub> is 7.5.<sup>11,12</sup> This is much higher than the one without amines (the concentration in MG<sub>non</sub> layers is 0.002 M). The high CO<sub>2</sub> concentration accelerated CO<sub>2</sub> permeation by driving CO<sub>2</sub> diffusion in the membranes. The selectivity of the MG<sub>non</sub> layer ( $\alpha_{\text{CO}_2/\text{N}_2} = 4$ ) might be due to different sorption coefficients of CO<sub>2</sub> and N<sub>2</sub> in the hydrated MG<sub>non</sub> layer.

It has been reported that hydrogel films consisting of MG<sub>Am</sub> can absorb ~3 mmol/g CO<sub>2</sub> by forming ammonium bicarbonate.<sup>11</sup> The amount of water required for 1 g of the MG<sub>Am</sub> layer to show a high CO<sub>2</sub> permeance is ~0.4 g (30 mmol/g; Figure 5B). This quantity is much larger than that required to form 3 mmol/g bicarbonate ions via an acid–base reaction (Figure 5C). These results suggest that the membrane should be hydrated not only to react with CO<sub>2</sub> to form ammonium bicarbonate but also for the bicarbonate ions to diffuse rapidly through the membrane.<sup>13</sup> It should be mentioned that the actual thickness of the MG layers at the working environment (95% RH) will be about 40% thicker than the thickness observed in SEM (dry state) based on the assumption that the density of the MG layers is the same as that of water.

### Facilitation of CO<sub>2</sub> Permeation.

Microgel membranes with high CO<sub>2</sub> selectivity can also be prepared by doping amines in the hydrogel layer to facilitate the acid–base reaction (Figure 5D,E). Microgels with carboxylic acid groups (denoted as MG<sub>CA</sub>) were prepared, as reported previously (Scheme 1),<sup>53</sup> and spray-coated on a porous support (26  $\mu\text{g}/\text{cm}^2$  on PES<sub>100</sub>) along with 2-(2-aminoethylamino)ethanol (AEE) (a well-studied amine with a high capacity for CO<sub>2</sub> absorption at a rapid rate).<sup>54</sup> Nitrogen permeation was adequately blocked by the MG<sub>CA</sub> layer (4 GPU), indicating that a defect-free layer was successfully formed by coating MG<sub>CA</sub> mixed with AEE onto PES<sub>100</sub>. The membrane showed a high and selective CO<sub>2</sub> permeance of 1010 GPU ( $\alpha_{\text{CO}_2/\text{N}_2} = 216$ ) against simulated post-combustion gases (10% CO<sub>2</sub>/90% N<sub>2</sub>, 64 °C, 85% RH) (Figure 5D). The purity of CO<sub>2</sub> in the permeate gas ([CO<sub>2</sub>]/([CO<sub>2</sub>] + [N<sub>2</sub>])) was >95%. Although helium sweep has to be

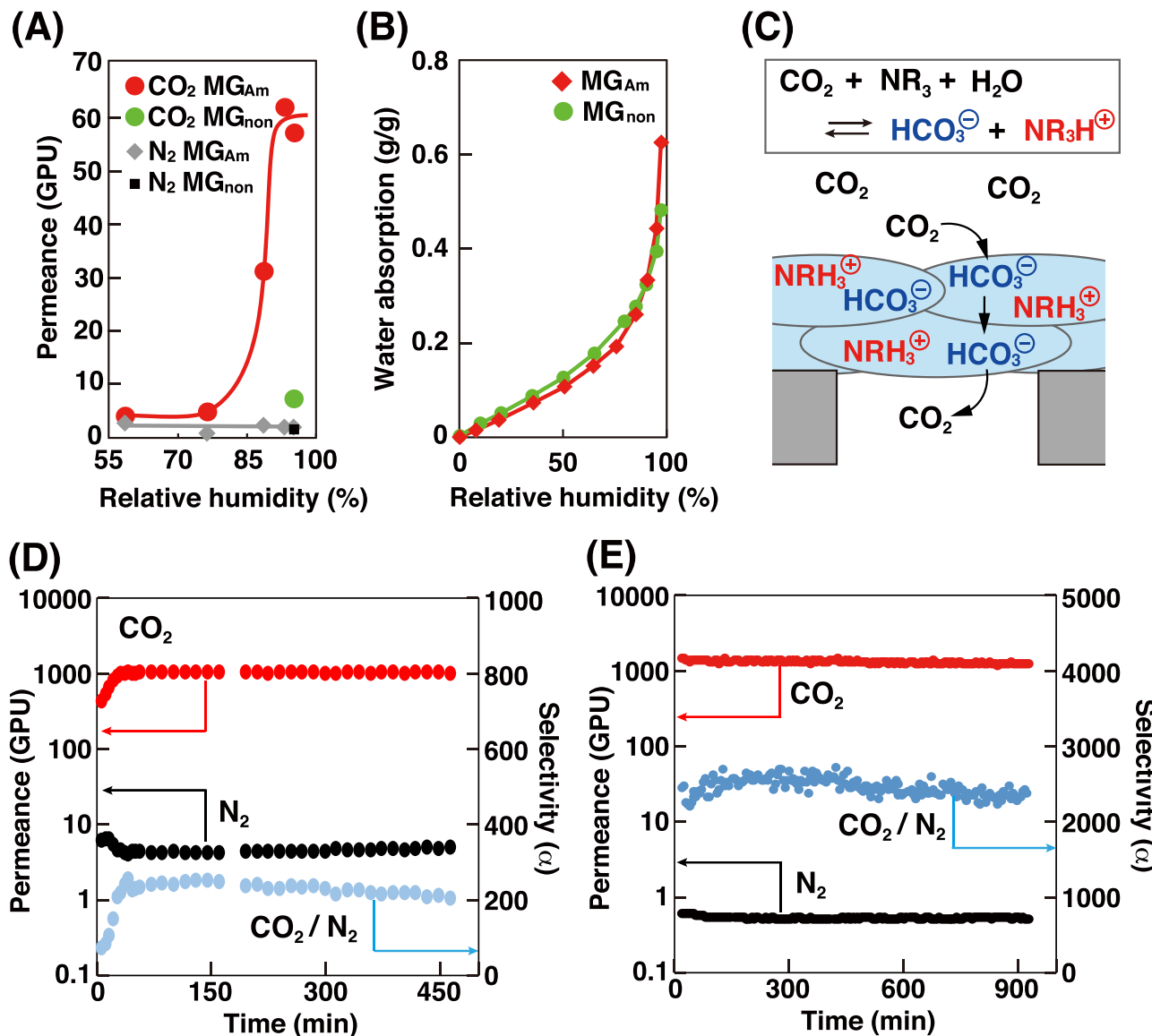


**Figure 5.**  $\text{CO}_2$ -separation performance of hydrogel membranes. (A) Effect of relative humidity (RH) on  $\text{CO}_2$  and  $\text{N}_2$  permeance of hydrogel membranes comprising amine-based microgels ( $\text{MG}_{\text{Am}}$ ) and amine-free microgels ( $\text{MG}_{\text{non}}$ ).  $\text{CO}_2$  and  $\text{N}_2$  permeance of  $\text{MG}_{\text{Am}}$  membranes are shown in red circles and gray diamonds, respectively.  $\text{CO}_2$  and  $\text{N}_2$  permeance of  $\text{MG}_{\text{non}}$  membranes are shown in green circles and black squares, respectively. (B) Effect of RH on water absorption by the hydrogel membranes comprising amine-based microgels ( $\text{MG}_{\text{Am}}$ ; red diamonds) and amine-free microgels ( $\text{MG}_{\text{non}}$ ; green circles). (C) Proposed mechanism of selective  $\text{CO}_2$  permeation through the amine-containing hydrogel layer assisted by reversible acid–base reaction and rapid diffusion of bicarbonate ions in the hydrogel layer. (D, E) Performance of amine-doped hydrogel membranes in the treatment of simulated post-combustion gases (D) (10 vol %  $\text{CO}_2$ /90 vol %  $\text{N}_2$ , 64 °C, 85% RH) and simulated atmospheric air (E) (400 ppm  $\text{CO}_2$ , 99.94 vol %  $\text{N}_2$ , 40 °C, 95% RH).

replaced by vacuum and/or steam sweep to actually purify  $\text{CO}_2$ ,<sup>55,56</sup> this  $\text{CO}_2$  permeance and selectivity are high enough to realize a single-stage, low-cost, and post-combustion  $\text{CO}_2$  capture process at point sources such as thermal power plants. The concentration of absorbed  $\text{CO}_2$  ( $\text{HCO}_3^-$  and  $\text{CO}_3^{2-}$ ) in the top side of the membrane (feed gas side) is calculated to be about 2 M, assuming that the reaction between amines and  $\text{CO}_2$  is equilibrated with the 10%  $\text{CO}_2$  feed gas (10 kPa) and  $pK_a$  of AEE is 9.<sup>12</sup> This is much higher than the one without AEE (concentrations in  $\text{MG}_{\text{Am}}$  and  $\text{MG}_{\text{non}}$  layers are 0.2 and 0.002 M, respectively). The high  $\text{CO}_2$  concentration facilitated  $\text{CO}_2$  permeation by driving  $\text{CO}_2$  diffusion in the membranes.

Further, the membranes showed a high  $\text{CO}_2$  permeance of 1270 GPU and a  $\alpha_{\text{CO}_2/\text{N}_2}$  of 2380 against simulated atmospheric air (400 ppm  $\text{CO}_2$ , 99.96%  $\text{N}_2$ , 40 °C, 95% RH) (Figure 5E).

The concentration of  $\text{CO}_2$  in the permeate gas was ~30%. Although helium sweep has to be replaced by vacuum and/or steam sweep to actually purify  $\text{CO}_2$ ,<sup>55,56</sup> this membrane enables low-cost direct  $\text{CO}_2$  capture from atmospheric air via a two-stage membrane separation process. The concentration of absorbed  $\text{CO}_2$  ( $\text{HCO}_3^-$  and  $\text{CO}_3^{2-}$ ) in the top side of the membrane is calculated to be 0.2 M, assuming that the equilibrium at 400 ppm  $\text{CO}_2$  feed gas (40 Pa) and  $pK_a$  of AEE is 9.<sup>12</sup> This is about 10 times lower than the concentration calculated in the post conditions (the concentration at 10%  $\text{CO}_2$  was 2 M). However,  $\text{CO}_2$  permeance is still high since the difference of  $\text{CO}_2$  partial pressure between the top side and back side of the membrane is much smaller (~40 Pa) under the conditions for direct  $\text{CO}_2$  capture than under the post-combustion conditions (~10 kPa).

## CONCLUSIONS

In this study, defect-free hydrogel nanomembranes were assembled by coating an aqueous suspension of microgels on the surface of a porous membrane. The deformability of the microgel particles enabled the autonomous assembly of a defect-free 30–50 nm-thick hydrogel layer consisting of two to three layers of ~15 nm-thick discoidal microgels. Microscopic analysis established that water penetration into the hydrophilic pores driven by capillary force assists the assembly of a dense defect-free microgel layer on the pores. This membrane formation mechanism provides insights into the self-assembly of soft materials.

The quartz crystal microbalance experiment clarified the importance of free water in the membranes for achieving fast diffusion of bicarbonate ions. The hydrogel nanomembranes consisting of amine-containing microgel particles exhibited selective CO<sub>2</sub> permeation (850 GPU,  $\alpha_{\text{CO}_2/\text{N}_2} = 25$ ) against post-combustion gases. Acid-containing microgel membranes doped with amines showed highly selective CO<sub>2</sub> permeation against post-combustion gases (1010 GPU,  $\alpha_{\text{CO}_2/\text{N}_2} = 216$ ) and direct air capture (1270 GPU,  $\alpha_{\text{CO}_2/\text{N}_2} = 2380$ ). The observed CO<sub>2</sub> permeance and selectivity are high enough to realize a single-stage, low-cost, and post-combustion CO<sub>2</sub> capture process at point sources such as thermal power plants and low-cost direct CO<sub>2</sub> capture from atmospheric air via a two-stage membrane separation process. Although the durability test as well as further efforts to design the membrane module and separation process is required, the versatile strategy of fabricating microgel nanomembranes by the autonomous assembly of deformable particles enables the large-scale manufacture of high-performance separation membranes and allows low-cost carbon capture from post-combustion gases and atmospheric air.

## ASSOCIATED CONTENT

### Supporting Information

The Supporting Information is available free of charge at <https://pubs.acs.org/doi/10.1021/acsami.1c06447>.

Supporting figures and experimental methods featuring SEM, TEM, elemental mapping, and other additional information found in this work ([PDF](#))

## AUTHOR INFORMATION

### Corresponding Author

**Yu Hoshino** — Department of Chemical Engineering, Faculty of Engineering, Kyushu University, Fukuoka 819-0395, Japan; Japan Carbon Cycle Lab., Inc., Fukuoka 819-0388, Japan; [orcid.org/0000-0001-9628-6979](https://orcid.org/0000-0001-9628-6979); Email: [yhoshino@chem-eng.kyushu-u.ac.jp](mailto:yhoshino@chem-eng.kyushu-u.ac.jp)

### Authors

**Tomohiro Gyobu** — Department of Chemical Engineering, Faculty of Engineering, Kyushu University, Fukuoka 819-0395, Japan

**Kazushi Imamura** — Department of Chemical Engineering, Faculty of Engineering, Kyushu University, Fukuoka 819-0395, Japan

**Akira Hamasaki** — Department of Chemical Engineering, Faculty of Engineering, Kyushu University, Fukuoka 819-0395, Japan

**Ryutaro Honda** — Department of Chemical Engineering, Faculty of Engineering, Kyushu University, Fukuoka 819-0395, Japan

**Ryoga Horii** — Department of Chemical Engineering, Faculty of Engineering, Kyushu University, Fukuoka 819-0395, Japan

**Chie Yamashita** — Department of Chemical Engineering, Faculty of Engineering, Kyushu University, Fukuoka 819-0395, Japan; Japan Carbon Cycle Lab., Inc., Fukuoka 819-0388, Japan

**Yuki Terayama** — Department of Chemical Engineering, Faculty of Engineering, Kyushu University, Fukuoka 819-0395, Japan

**Takeshi Watanabe** — Department of Chemical Engineering, Faculty of Engineering, Kyushu University, Fukuoka 819-0395, Japan; Japan Carbon Cycle Lab., Inc., Fukuoka 819-0388, Japan

**Shoma Aki** — Department of Chemical Engineering, Faculty of Engineering, Kyushu University, Fukuoka 819-0395, Japan; Japan Carbon Cycle Lab., Inc., Fukuoka 819-0388, Japan

**Yida Liu** — Department of Chemical Engineering, Faculty of Engineering, Kyushu University, Fukuoka 819-0395, Japan

**Junko Matsuda** — International Institute for Carbon-Neutral Energy Research (WPI-I2CNER), Kyushu University, Fukuoka 819-0395, Japan; International Research Center for Hydrogen Energy, Kyushu University, Fukuoka 819-0395, Japan; [orcid.org/0000-0002-5962-4139](https://orcid.org/0000-0002-5962-4139)

**Yoshiko Miura** — Department of Chemical Engineering, Faculty of Engineering, Kyushu University, Fukuoka 819-0395, Japan; [orcid.org/0000-0001-8590-6079](https://orcid.org/0000-0001-8590-6079)

**Ikuo Taniguchi** — International Institute for Carbon-Neutral Energy Research (WPI-I2CNER), Kyushu University, Fukuoka 819-0395, Japan; [orcid.org/0000-0001-7644-8723](https://orcid.org/0000-0001-7644-8723)

Complete contact information is available at:  
<https://pubs.acs.org/10.1021/acsami.1c06447>

### Author Contributions

The manuscript was written through contributions of all authors. All authors have given approval to the final version of the manuscript.

### Funding

This research was supported by JST ALCA, Japan (grant no. JPMJAL1403) and the Japan Aerospace Exploration Agency (JAXA) Open Innovation Hub Center.

### Notes

The authors declare no competing financial interest.

## REFERENCES

- (1) Bui, M.; Adjiman, C. S.; Bardow, A.; Anthony, E. J.; Boston, A.; Fennell, S. B. P. S.; Fuss, S.; Galindo, A.; Hackett, L. A.; Hallett, J. P.; Herzog, H. J.; Jackson, G.; Kemper, J.; Krevor, S.; Maitland, G. C.; Matuszewski, M.; Metcalfe, I. S.; Petit, C.; Puxty, G.; Reimer, J.; Reiner, D. M.; Rubin, E. S.; Scott, S. A.; Shah, N.; Smit, B.; Trusler, J. P. M.; Webley, P.; Wilcoxon, J.; Mac Dowell, N. Carbon Capture and Storage (CCS): The Way Forward. *Energy Environ. Sci.* **2018**, *11*, 1062–1176.
- (2) Sanz-Perez, E. S.; Murdock, C. R.; Didas, S. A.; Jones, C. W. Direct Capture of CO<sub>2</sub> from Ambient Air. *Chem. Rev.* **2016**, *116*, 11840–11876.
- (3) Goeppert, A.; Czaun, M.; Prakash, G. K. S.; Olah, G. A. Air as the Renewable Carbon Source of the Future: An Overview of CO<sub>2</sub> Capture from the Atmosphere. *Energy Environ. Sci.* **2012**, *5*, 7833–7853.
- (4) Park, H. B.; Kamcev, J.; Robeson, L. M.; Elimelech, M.; Freeman, B. D. Maximizing the Right Stuff: The Trade-Off Between Membrane Permeability and Selectivity. *Science* **2017**, *356*, No. eaab0530.

- (5) Merkel, T. C.; Lin, H.; Wei, X.; Baker, R. Power Plant Post-Combustion Carbon Dioxide Capture: An Opportunity for Membranes. *J. Membr. Sci.* **2010**, *359*, 126–139.
- (6) Du, N.; Park, H. B.; Dal-Cin, M. M.; Guiver, M. D. Advances in High Permeability Polymeric Membrane Materials for CO<sub>2</sub> Separation. *Energy Environ. Sci.* **2012**, *5*, 7306–7322.
- (7) Sagle, A. C.; Ju, H.; Freeman, B. D.; Sharma, M. M. PEG-Based Hydrogel Membrane Coatings. *Polymer* **2009**, *50*, 756–766.
- (8) Ju, H.; Sagle, A. C.; Freeman, B. D.; Mardel, J. I.; Hill, A. J. Characterization of Sodium Chloride and Water Transport in Crosslinked Poly(Ethylene Oxide) Hydrogels. *J. Membr. Sci.* **2010**, *358*, 131–141.
- (9) Wu, Y.; Joseph, S.; Aluru, N. R. Effect of Cross-Linking on the Diffusion of Water, Ions, and Small Molecules in Hydrogels. *J. Phys. Chem. B* **2009**, *113*, 3512–3520.
- (10) Liu, Y.; Yu, S.; Wu, H.; Li, Y.; Wang, S.; Tian, Z.; Jiang, Z. High Permeability Hydrogel Membranes of Chitosan/Poly Ether-Block-Amide Blends for CO<sub>2</sub> separation. *J. Membr. Sci.* **2014**, *469*, 198–208.
- (11) Yue, M.; Hoshino, Y.; Miura, Y. Design Rationale of Thermally Responsive Microgel Particle Films that Reversibly Absorb Large Amounts of CO<sub>2</sub>: Fine Tuning the pK<sub>a</sub> of Ammonium Ions in the Particles. *Chem. Sci.* **2015**, *6*, 6112–6123.
- (12) Honda, R.; Hamasaki, A.; Miura, Y.; Hoshino, Y. Thermoresponsive CO<sub>2</sub> Absorbent for Various CO<sub>2</sub> Concentrations: Tuning the pK<sub>a</sub> of Ammonium Ions for Effective Carbon Capture. *Polym. J.* **2021**, *53*, 157–167.
- (13) Zhang, X.; Chen, L.; Lim, K. H.; Gonuguntla, S.; Lim, K. W.; Pranantyo, D.; Yong, W. P.; Yam, W. J. T.; Low, Z.; Two, W. J.; Nien, H. P.; Loh, Q. W.; Soh, S. The Pathway to Intelligence: Using Stimuli-Responsive Materials as Building Blocks for Constructing Smart and Functional Systems. *Adv. Mater.* **2019**, *31*, 1804540.
- (14) Yue, M.; Hoshino, Y.; Ohshiro, Y.; Imamura, K.; Miura, Y. Temperature-responsive Microgel Films as Reversible Carbon Dioxide Absorbents in Wet Environment. *Angew. Chem., Int. Ed.* **2014**, *53*, 2654–2657.
- (15) Kim, H. W.; Yoon, H. W.; Yoon, S.-M.; Yoo, B. M.; Ahn, B. K.; Cho, Y. H.; Shin, H. J.; Yang, H.; Paik, U.; Kwon, S.; Choi, J.-Y.; Park, H. B. Selective Gas Transport Through Few-Layered Graphene and Graphene Oxide Membranes. *Science* **2013**, *342*, 91–95.
- (16) Peng, Y.; Li, Y.; Ban, Y.; Jin, H.; Jiao, W.; Liu, X.; Yang, W. Metal-Organic Framework Nanosheets as Building Blocks for Molecular Sieving Membranes. *Science* **2014**, *346*, 1356–1359.
- (17) Jimenez-Solomon, M. F.; Song, Q.; Jelfs, K. E.; Munoz-Ibanez, M.; Livingston, A. G. Polymer Nanofilms with Enhanced Microporosity by Interfacial Polymerization. *Nat. Mater.* **2016**, *15*, 760–767.
- (18) Chen, Y.; Ho, W. S. W. High-Molecular-Weight Polyvinylamine/Piperazine Glycinate Membranes for CO<sub>2</sub> Capture from Flue Gas. *J. Membr. Sci.* **2016**, *514*, 376–384.
- (19) Qiao, Z.; Zhao, S.; Sheng, M.; Wang, J.; Wang, S.; Wang, Z.; Zhong, C.; Guiver, M. D. Metal-Induced Ordered Microporous Polymers for Fabricating Large-Area Gas Separation Membranes. *Nat. Mater.* **2018**, *18*, 163–168.
- (20) Jeon, M. Y.; Kim, D.; Kumar, P.; Lee, P. S.; Rangnekar, N.; Bai, P.; Shete, M.; Elyassi, B.; Lee, H. S.; Narasimharao, K.; Basahel, S. N.; Al-Thabaiti, S.; Xu, W.; Cho, H. J.; Fetisov, E. O.; Thyagarajan, R.; DeJaco, R. F.; Fan, W.; Mkhdyan, K. A.; Siepmann, J. I.; Tsapatsis, M. Ultra-Selective High-Flux Membranes from Directly Synthesized Zeolite Nanosheets. *Nature* **2017**, *543*, 690–694.
- (21) Vendamme, R.; Onoue, S.-Y.; Nakao, A.; Kunitake, T. Robust Free-Standing Nanomembranes of Organic/Inorganic Interpenetrating Networks. *Nat. Mater.* **2006**, *5*, 494–501.
- (22) Fu, Y.; Jiang, Y.-B.; Dunphy, D.; Xiong, H.; Coker, E.; Chou, S. S.; Zhang, H.; Vanegas, J. M.; Croissant, J. G.; Cecchi, J. L.; Rempe, S. B.; Brinker, C. J. Ultra-Thin Enzymatic Liquid Membrane for CO<sub>2</sub> Separation and Capture. *Nat. Commun.* **2018**, *9*, 990.
- (23) Du, Y.; Lo, E.; Ali, S.; Khademhosseini, A. Directed Assembly of Cell-Laden Microgels for Fabrication of 3D Tissue Constructs. *Proc. Natl. Acad. Sci.* **2008**, *105*, 9522–9527.
- (24) Qi, H.; Ghodousi, M.; Du, Y.; Grun, C.; Bae, H.; Yin, P.; Khademhosseini, A. DNA-Directed Self-Assembly of Shape-Controlled Hydrogels. *Nat. Commun.* **2013**, *4*, 2275.
- (25) Malda, J.; Visser, J.; Melchels, F. P.; Jüngst, T.; Hennink, W. E.; Dherf, W. J. A.; Groll, J.; Hutmacher, D. W. 25th Anniversary Article: Engineering Hydrogels for Biofabrication. *Adv. Mater.* **2013**, *25*, S011–S028.
- (26) Hong, S.; Sycks, D.; Chan, H. F.; Lin, S.; Lopez, G. P.; Guilak, F.; Leong, K. W.; Zhao, X. 3D Printing of Highly Stretchable and Tough Hydrogels into Complex, Cellularized Structures. *Adv. Mater.* **2015**, *27*, 4035–4040.
- (27) Gladman, A. S.; Matsumoto, E. A.; Nuzzo, R. G.; Mahadevan, L.; Lewis, J. A. Biomimetic 4D Printing. *Nat. Mater.* **2016**, *15*, 413–418.
- (28) Zhang, Y. S.; Khademhosseini, A. Advances in Engineering Hydrogels. *Science* **2017**, *356*, No. eaaf3627.
- (29) Beebe, D. J.; Moore, J. S.; Bauer, J. M.; Yu, Q.; Liu, R. H.; Devadoss, C.; Jo, B.-H. Functional Hydrogel Structures for Autonomous Flow Control Inside Microfluidic Channels. *Nature* **2000**, *404*, 588–590.
- (30) Sidorenko, A.; Krupenkin, T.; Taylor, A.; Fratzl, P.; Aizenberg, J. Reversible Switching of Hydrogel-Actuated Nanostructures into Complex Micropatterns. *Science* **2007**, *315*, 487–490.
- (31) Plamper, F. A.; Richtering, W. Functional Microgels, and Microgel Systems. *Acc. Chem. Res.* **2017**, *50*, 131–140.
- (32) Karg, M.; Pich, A.; Hellweg, T.; Hoare, T.; Lyon, L. A.; Crassous, J. J.; Suzuki, D.; Gumerov, R. A.; Schneider, S.; Potemkin, I. I.; Richtering, W. Nanogels and Microgels: From Model Colloids to Applications, Recent Developments, and Future Trends. *Langmuir* **2019**, *35*, 6231–6255.
- (33) Scotti, A.; Gasser, U.; Herman, E. S.; Pelaez-Fernandez, M.; Han, J.; Menzel, A.; Lyon, L. A.; Fernández-Nieves, A. The Role of Ions in the Self-Healing Behavior of Soft Particle Suspensions. *Proc. Natl. Acad. Sci. U. S. A.* **2016**, *113*, 5576–5581.
- (34) South, A. B.; Lyon, L. A. Autonomic Self-Healing of Hydrogel Thin Films. *Angew. Chem., Int. Ed.* **2010**, *122*, 779–783.
- (35) Luo, F.; Xie, R.; Liu, Z.; Ju, X.-J.; Wang, W.; Lin, S.; Chu, L.-Y. Smart Gating Membranes with *In Situ* Self-Assembled Responsive Nanogels as Functional Gates. *Sci. Rep.* **2015**, *5*, 14708.
- (36) Csetnek, I.; Filipcsei, G.; Zrínyi, M. Smart Nanocomposite Polymer Membranes with On/Off Switching Control. *Macromolecules* **2006**, *39*, 1939–1942.
- (37) Zhang, K.; Huang, H.; Yang, G.; Shaw, J.; Yip, C.; Wu, X. Y. Characterization of Nanostructure of Stimuli-Responsive Polymeric Composite Membranes. *Biomacromolecules* **2004**, *5*, 1248–1255.
- (38) Bell, D. J.; Ludwanowski, S.; Lüken, A.; Sarikaya, B.; Walther, A.; Wessling, M. Hydrogel Membranes Made from Crosslinked Microgel Multilayers with Tunable Density. *J. Membr. Sci.* **2021**, *620*, 118912.
- (39) Wiese, M.; Lohaus, T.; Haussmann, J.; Wessling, M. Charged Microgels Adsorbed on Porous Membranes - A Study of Their Mobility and Molecular Retention. *J. Membr. Sci.* **2019**, *588*, 117190.
- (40) Barth, M.; Wiese, M.; Ogieglo, W.; Go, D.; Kuehne, A. J. C.; Wessling, M. Monolayer Microgel Composite Membranes with Tunable Permeability. *J. Membr. Sci.* **2018**, *555*, 473–482.
- (41) Menne, D.; Pitsch, F.; Wong, J. E.; Pich, A.; Wessling, A. Temperature-Modulated Water Filtration Using Microgel-Functionalized Hollow-Fiber Membranes. *Angew. Chem., Int. Ed.* **2014**, *53*, 5706–5710.
- (42) Tripathi, B. P.; Dubey, N. C.; Stamm, M. Hollow Microgel Based Ultrathin Thermoresponsive Membranes for Separation, Synthesis, and Catalytic Applications. *ACS Appl. Mater. Interfaces* **2014**, *6*, 17702–17712.
- (43) Lohaus, T.; de Wit, P.; Kather, M.; Menne, D.; Benes, N. E.; Pich, A.; Wessling, M. Tunable Permeability and Selectivity: Heatable Inorganic Porous Hollow Fiber Membrane with a Thermo-Responsive Microgel Coating. *J. Membr. Sci.* **2017**, *539*, 451–457.
- (44) Hoshino, Y.; Imamura, K.; Yue, M.; Inoue, G.; Miura, Y. Reversible Absorption of CO<sub>2</sub> Triggered by Phase Transition of Amine-Containing Micro- and Nano-Gel Particles. *J. Am. Chem. Soc.* **2012**, *134*, 18177–18180.

- (45) van de Wetering, P.; Moret, E. E.; Schuurmans-Nieuwenbroek, N. M. E.; van Steenbergen, M. J.; Hennink, W. E. Structure-Activity Relationships of Water-Soluble Cationic, Methacrylate/Methacrylamide Polymers for Nonviral Gene Delivery. *Bioconjugate Chem.* **1999**, *10*, 589–597.
- (46) Vogelaar, L.; Barsema, J. N.; van Rijn, C. J. M.; Nijdam, W.; Wessling, M. Phase Separation Micromolding—PS $\mu$ M. *Adv. Mater.* **2003**, *15*, 1385–1389.
- (47) Peters, A. M.; Lammertink, R. G. H.; Wessling, M. Comparing Flat and Micro-Patterned Surfaces: Gas Permeation and Tensile Stress Measurements. *J. Membr. Sci.* **2008**, *320*, 173–178.
- (48) Picard, C.; Garrigue, P.; Tatry, M.-C.; Lapeyre, V.; Ravaine, S.; Schmitt, V.; Ravaine, V. *Langmuir* **2017**, *33*, 7968–7981.
- (49) Minato, H.; Murai, M.; Watanabe, T.; Matsui, S.; Takizawa, M.; Kureha, T.; Suzuki, D. The Deformation of Hydrogel microspheres at the Air/Water Interface. *Chem. Commun.* **2018**, *54*, 932–935.
- (50) Hao, P.; Wijmans, J. G.; He, Z.; White, L. S. Effect of Pore Location and Pore Size of the Support Membrane on the Permeance of Composite Membranes. *J. Membr. Sci.* **2020**, *594*, 117465.
- (51) Hernández, A.; Calvo, J. I.; Prádanos, P.; Palacio, L.; Rodríguez, M. L.; de Saja, J. A. Surface Structure of Microporous Membranes by Computerized SEM Image Analysis Applied to Anopore Filters. *J. Membr. Sci.* **1997**, *137*, 89–97.
- (52) Hendrickson, G. R.; Lyon, L. A. Microgel Translocation through Pores under Confinement. *Angew. Chem., Int. Ed.* **2010**, *49*, 2193–2197.
- (53) Hoshino, Y.; Moribe, M.; Gondo, N.; Jibiki, T.; Nakamoto, M.; Guo, B.; Adachi, R.; Miura, Y. Combining Acid- and Base-Imprinted Nanoparticles in a Hydrogel Film for Temperature-Responsive Quick and Reversible Capture of Salt. *ACS Appl. Polym. Mater.* **2020**, *2*, 505–514.
- (54) Bonenfant, D.; Mimeault, M.; Hausler, R. Comparative Analysis of the Carbon Dioxide Absorption and Recuperation Capacities in Aqueous 2-(2-Aminoethylamino)ethanol (AEE) and Blends of Aqueous AEE and *N*-Methyldiethanolamine Solutions. *Ind. Eng. Chem. Res.* **2005**, *44*, 3720–3725.
- (55) Vakharia, V.; Salim, W.; Gasda, M.; Ho, W. S. W. Oxidatively stable membranes for CO<sub>2</sub> separation and H<sub>2</sub> purification. *J. Membr. Sci.* **2017**, *533*, 220–228.
- (56) Fujiki, J.; Chowdhury, F. A.; Yamada, H.; Yogo, K. Highly efficient post-combustion CO<sub>2</sub> capture by low-temperature steam-aided vacuum swing adsorption using a novel polyamine-based solid sorbent. *Chem. Eng. J.* **2017**, *307*, 273–282.